Toward Real-time 3D Ultrasound Registration-based Visual Servoing for Interventional Navigation

Oliver Zettinig[1,2], Bernhard Fuerst[1,2], Risto Kojcev[2,3], Marco Esposito[1], Mehrdad Salehi[4], Wolfgang Wein[4], Julia Rackerseder[1], Edoardo Sinibaldi[3], Benjamin Frisch[1], Nassir Navab[1,2]

***Abstract*— While intraoperative imaging is commonly used to guide surgical interventions, automatic robotic support for image-guided navigation has not yet been established in clinical routine. In this paper, we propose a novel visual servoing framework that combines, for the first time, full image-based 3D ultrasound registration with a real-time servo-control scheme. Paired with multi-modal fusion to a pre-interventional plan such as an annotated needle insertion path, it thus allows tracking a target anatomy, continuously updating the plan as the target moves, and keeping a needle guide aligned for accurate manual insertion. The presented system includes a motorized 3D ultrasound transducer mounted on a force-controlled robot and a GPU-based image processing toolkit. The tracking accuracy of our framework is validated on a geometric agar/gelatin phantom using a second robot, achieving positioning errors of on average 0.42±0.44 mm. With compounding and registration runtimes of up to total around 550 ms, real-time performance comes into reach. We also present initial results on a spine phantom, demonstrating the feasibility of our system for lumbar spine injections.**

I. INTRODUCTION

Ultrasound (US) has become a standard diagnostic and guidance modality in many clinical fields, especially because of its low cost, lack of ionizing radiation and ease of use in interventional settings. In particular, US is real-time and therefore allows for movement-independent guidance. However, the exclusive use of US imaging has not become standard of care for many interventions. In this work, we focus on needle injections in the lumbar spine [1], for which guidance with X-ray fluoroscopy is currently recommended [2]. But also in other fields, such as electrode placement for deep brain stimulation [3], or cardiac catheter placement [4], US guidance has not yet reached maturity. In these scenarios, lower image quality, limited view of the anatomy and higher difficulty in interpreting the images are regularly identified as challenges in guaranteeing accurate placement [2]. In addition, manually navigating the transducer to the correct site and maintaining a suitable acoustic window has been reported cumbersome and linked to a steep learning curve [5].

In recent years, several techniques have been proposed to tackle a subset of these limitations. Real-time guidance can be achieved by optical or electromagnetic tracking of a freehand US transducer and initial registration to a pre-interventional CT or MR image (as in [6], [7], [8] and [9]), or an atlas of the spine [10]. Once the registration is established, and as long as the patient does not move, the contours of the vertebrae can be highlighted, and the insertion path of a tool, which is also tracked, visualized. Brudfors et al. [11] utilized such an atlas and presented again a tracker-less guidance system for spine anaesthesia. In their study, a statistical spine model is continuously registered to and overlaid on live 3D US volumes together with a calibrated needle guide line.

Aforementioned works share the common disadvantage that the physician is required to manually maintain sufficient image quality using a handheld US transducer. Hence, several robot-assisted systems incorporating a visual servo-control scheme based on features derived from the live 2D or 3D US images have been proposed in the last decade. Exemplary applications include in-plane [12] and out-of-plane [13] carotid artery tracking, compensation of organ motion [14], and maintenance of visibility in tele-operated settings [15]. In a variety of works, graphics hardware is exploited for real-time processing of US images, including motion detection with strain imaging [16].

The vast majority of prior art on ultrasound servoing tackles the issue of needle tracking and steering, regularly relying on a static US probe, see [17] and [18]. Nevertheless, as necessary control schemes translate seamlessly to systems where the US transducer itself is steered by the robot, progress has been made toward full automation of specific parts of certain surgeries. Nadeau et al. [19] have shown that real-time visual servoing for both instrument and anatomy tracking for reasonably small regions of interest is feasible.

To the best of our knowledge, fully employing complete image-based 3D-to-3D volume registration in the scope of US transducer visual servoing has not been performed yet. In this work, we propose a novel robotic visual servoing framework based on 3D ultrasound images that continuously re-registers the live image stream with an interventional plan. Derived using multi-modal image registration, such a plan is based on annotions on pre-interventional CT or MR images. The rigid transformation found by the registration algorithm directly serves as signal for servo-control. Any movement of the target anatomy therefore leads to an adjustment of the pose of the US transducer. Thus, our framework does not only release the physician from holding the US probe, but at the same time provides continuous guidance even if the target moves.

This work is partially supported by the Bayerische Forschungsstiftung award number AZ-1072-13 (RoBildOR).

[1] Computer Aided Medical Procedures, Technische Universität München, Munich, Germany. oliver.zettinig@tum.de

[2] Computer Aided Medical Procedures, Johns Hopkins University, Baltimore, MD, USA

[3] Micro-Biorobotics, Istituto Italiano di Tecnologia, Pontedera, Italy.

[4] ImFusion GmbH, Munich, Germany.

978-1-4673-8026-3/16/$31.00

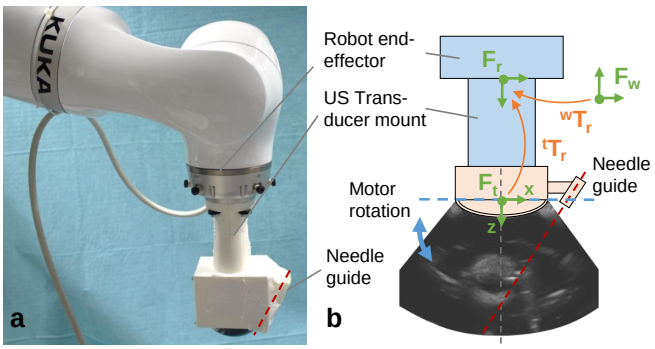

Fig. 1. **a)** System design including robot, mount, needle guide, and motorized US transducer. **b)** Schematic showing used world (F_w), robot end-effector (F_r) and US transducer (F_t) coordinate frames as well as the transformations between them. *See text for details.*

II. METHODS

Our interventional navigation system utilizes a robot with seven degrees of freedom, equipped with torque sensors at each joint, and an US transducer rigidly attached to its end-effector (see Fig. 1a). The robot is controlled following the system architecture illustrated in Fig. 2. The two-layer concept reflects the proposed combination of intensity-based image registration and visual servoing. In an outer control loop, each incoming 3D US image is registered to an intial scan. The resulting transformation to align these two images is utilized to update the desired pose of the US transducer, thus following a moving target anatomy. An inner control loop implements an indirect, compliant force control scheme, maintaining a constant contact force onto the patient. This does not only ensure sufficient image quality but also tackles patient safety concerns. After describing the control laws for both loops in Sec. II-A/B, the alignment to a planned needle path is explained in Sec. II-C.

A. Impedance Control Scheme

The employed impedance control aims at establishing a mass-damper-spring relation between the Cartesian end-effector position and an external force F_{ext}, measured using the robot configuration and the joint torque sensors. The intended behavior of our force controller is to balance F_{ext} to a desired end-effector force F_d, i.e. $F_{ext} - F_d = 0$. Briefly summarizing the control scheme by Albu-Schäffer et al. [20], the command joint torques τ_{cmd} are determined as follows:

$$\tau_{cmd} = \mathrm{J}(q)^\intercal \left[F_d - \mathrm{K}\Delta x - \mathrm{D}\Delta\dot{x}\right] + f_{idyn}(q, \dot{q}, \ddot{q}). \quad (1)$$

Hereby, $\mathrm{J}(q)$ denotes the Jacobian matrix, K and D positive definite damping and stiffness matrices, respectively, and $\Delta x = x_m - x_d$ the Cartesian position error between desired (x_d) and actual position (x_m). $f_{idyn}(q, \dot{q}, \ddot{q})$ is the solution of the inverse dynamics system without external influence.

B. Visual Control Scheme

The aim of the visual servoing controller is to compensate for target anatomy motion, which is visible through 3D US imaging. To quantify the misalignment of an initial image I_0, obtained at the beginning of the procedure, and the current image I_i, one could define the visual error e_v using an intensity-based similarity function: $e_v = 1 - S(\mathrm{I}_i, \mathrm{I}_0)$, assuming $S(\mathrm{I}, \mathrm{I}) = 1$. It is, however, more helpful to directly estimate a transformation $\hat{T}_i$ that will align the initial image with the current one:

$$\hat{\mathrm{T}}_i = \begin{pmatrix} \mathrm{R}(\alpha, \beta, \gamma) & (t_x, t_y, t_z)^\intercal \\ 0 & 1 \end{pmatrix} = \arg\max_T S(\mathrm{I}_i, T(\mathrm{I}_0)). \quad (2)$$

Throughout this paper, all transformations and vectors are expressed in computer vision notation, i.e. using 4×4 homogeneous matrices and 4×1 vectors. For the rigid case, based on the assumption of locally rigid movements [21], the transformation parameters $(t_x, t_y, t_z, \alpha, \beta, \gamma)$ constitute six degrees of freedom. As both images are US volumes, normalized cross correlation (NCC) is a suitable choice for the similarity function S in our framework [21]:

$$S(\mathrm{A}, \mathrm{B}) = \frac{1}{N} \sum_{j=1}^{N} \frac{(\mathrm{A}_j - \bar{\mathrm{A}})(\mathrm{B}_j - \bar{\mathrm{B}})}{\sigma_\mathrm{A} \sigma_\mathrm{B}}, \quad (3)$$

where N is the size of the overlapping, non-masked area of both images, A_j the intensity in image A of the j-th voxel of that area, $\bar{\mathrm{A}}$ the mean intensity of image A, and σ_A its standard deviation (analogous for image B). Intensity-based registration is ultimately to be preferred, since it both considers the entire available image content, and at the same time avoids the pitfalls of additional errors which may be introduced in feature selection and extraction steps. Note that the current image I_i is the fixed image, because it is embedded in the world coordinate frame. The evaluation can be efficiently implemented on the GPU, and the optimization of the parameters is performed using BOBYQA [22].

To avoid that both controllers act along the same axes, the degrees of freedom of the optimization procedure are restricted, in particular along the z-axis of frame F_t. This ensures that the force control on the tissue is not restrained by desired position updates. Note that additional degrees of freedom might be excluded by the user from the optimization for speed-up, for instance if only translations are expected.

The visual control law then determines a new, desired Cartesian pose for the US transducer $x_{d_i} = ({}^t\mathrm{T}_r)^{-1} \cdot (\hat{\mathrm{T}}_i)^{-1} \cdot \vec{o}_i$, where ${}^t\mathrm{T}_r$ is the extrinsic calibration between robot

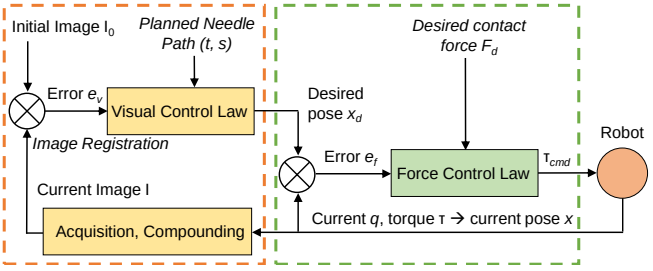

Fig. 2. Two-layer robot control architecture. While the visual servoing part computes new Cartesian robot poses based on 3D US image registration, the impedance-based force controller balances desired transducer positions and required contact forces.

end-effector and US transducer, and $\vec{o}_i$ the origin of the current US image, i.e. the origin of frame F_t at the time of acquisition. For the next step $(i+1)$, the registration is initialized with $\hat{\mathrm{T}}_i$.

C. Needle Guide Control Scheme

To align the needle guide such that a predefined target is hit, more constraints have to be taken into account. Hence, the workflow becomes slightly more complex: First, a needle target point t_0, a suitable insertion path $\vec{s}_0$, and an intended US plane for image guidance are defined in a pre-interventional (CT or MR) image I_p. It is automatically registered to the initial US image I_0 as follows: $\hat{\mathrm{T}}_{pre} = \arg\max_T S_p(\mathrm{I}_0, T(\mathrm{I}_p))$, where S_p is the multi-modal LC^2 similarity metric [23]. To avoid misregistration because of local minima due to the ambiguity of vertebrae, manual initialization might be necessary. The resulting transformation $\hat{\mathrm{T}}_{pre}$ embeds I_p and its annotations into the world coordinate frame F_w.

During the whole intervention, images I_i and I_0 are continuously registered as explained above. The annotations are carried along as the target anatomy might move: $t_i = (\hat{\mathrm{T}}_i)^{-1}\hat{\mathrm{T}}_{pre} \cdot t_0$; $\vec{s}_i = (\hat{\mathrm{T}}_i)^{-1}\hat{\mathrm{T}}_{pre} \cdot \vec{s}_0$. However, instead of directly using $\hat{\mathrm{T}}_i$ to compute a new desired pose, the current position of the needle guide line is now considered. Let n_i and m_i be the two calibrated needle points in frame F_w, i.e. two points the needle would hit if inserted, and $\vec{l}_i = (m_i - n_i)/\|m_i - n_i\|$ the normalized needle guide direction, as illustrated in Fig. 3. The necessary correction to make $\vec{s}_i$ and $\vec{l}_i$ parallel is then the rotation around axis $\vec{s}_i \times \vec{l}_i$ by angle $\mathrm{acos}(\langle \vec{s}_i, \vec{l}_i \rangle)$, denoted C_i. To make both lines coincide, an additional offset orthogonal to $\vec{s}_i$ is required: $\vec{u}_i = (m_i - t_i) - \vec{s}_i \cdot \langle \vec{s}_i, m_i - t_i \rangle$. Incorporating these two corrections in matrix

$$\mathrm{H}_i = \begin{pmatrix} \mathrm{C}_i & \vec{u}_i \\ 0 & 1 \end{pmatrix}, \tag{4}$$

the new pose for the US transducer can be determined by the modified visual control law as $x_{d_i} = ({}^t\mathrm{T}_r)^{-1} \cdot \mathrm{H}_i \cdot (\hat{\mathrm{T}}_i)^{-1} \cdot \vec{o}_i$. The behavior induced by this control law serves two purposes: (1) The target anatomy (and thus also the defined injection target), are tracked and will be followed as they move. (2) The calibrated needle guide will be aligned with the defined needle insertion path. Note that due to the impedance behavior of the system, the physician manually inserting the needle can push the needle guide into all directions to perform slight adjustments, if necessary.

III. SYSTEM SETUP

A. Hardware

For B-mode US acquisition, an Ultrasonix® Sonix RP system with a motorized curvilinear transducer m4DC7-3/40 is used (Ultrasonix Medical Corp., Richmond, BC, Canada). The acquisition rate is 30 Hz, the frequency chosen to be 3.3 MHz, the depth is set to 70 mm, and the gain to 50%. Similar to [11], the speed of the motor is defined such that a volume update rate of 1.3 Hz is achieved, each covering a sweep of $\pm 30°$.

As illustrated in Fig. 1a, the employed manipulator is a KUKA® LBR iiwa 7 R800 robot (KUKA Roboter GmbH, Augsburg, Germany), to whose end-effector a custom 3D-printed mount for the US transducer is fixed. The mount also incorporates a needle guide similar to the EpiGuide system [24] to fully exploit the targeting capabilities of the robot. A KUKA Sunrise Connectivity SmartServo application, similar to the approach in [25], is utilized to control the robot via OpenIGTLink commands directly on the robot controller machine. The application is based on the impedance control capabilities of the SmartServo library.

B. 3D Image Acquisition

3D US volumes are acquired using the publicly available PLUS library 2.2.0 [26], which in turn relies on the Ultrasonix Porta SDK 5.75. Running directly on the US machine, 2D frames in the transducer coordinate frame F_t (see Fig. 1b) are sent via Ethernet and the OpenIGTLink protocol [27] to a client workstation (Intel® Core i7-4770K processor at 3.5 GHz, 32 GB RAM, NVIDIA® GeForce GTX 770 graphics card). The intrinsic calibration between F_t and the US image coordinate system is determined using the imaging parameters provided by the US system (known spacing and pixel coordinates of the first center US ray sample) and the current motor position.

ImFusion Suite 1.1.8 (ImFusion GmbH, Munich, Germany), is an extendible GPU-based image processing framework for medical images. Two instances of the OpenIGTLink plugin maintain Ethernet connections to both the robot controller and the ultrasound system. Implementing a backward warping strategy as in [28], the incoming B-mode 2D images are compounded on the GPU into volumes with an isometric resolution of 0.3 mm, and placed into the world coordinate system F_w. The extrinsic calibration ${}^t\mathrm{T}_r$ to the end effector is easily found using the CAD design of the probe and the mount, and the transformation ${}^w\mathrm{T}_r$ is the current end-effector pose provided by the robot. Knowing the full chain of transformations, the rigidly attached needle guide can be calibrated in water by manually identifying two needle points n_0 and m_0 in the F_t frame. All image registration steps are implemented as ImFusion Suite plugin.

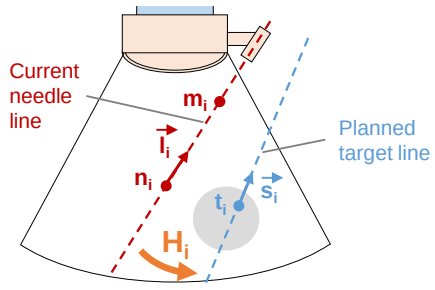

Fig. 3. To allow robotic needle guidance, the visual control law needs to bring the current needle guide line (red, $\vec{l}_i$) and the planned insertion path (blue, $\vec{s}_i$), two skew lines, into alignment. *See text for details.*

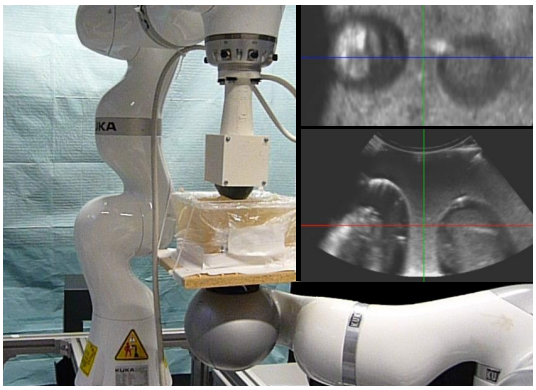

Fig. 5. Setup for tracking accuracy validation experiments. A second robot is holding a gelatin/agar phantom with spherical targets. Inlets show coronal (*top*) and axial (*bottom*) slices of the compounded 3D US volume.

IV. EXPERIMENTS

A. Tracking Accuracy Validation

For all our experiments, agar and gelatin phantoms [29] were used to create suitable tissue contrast in ultrasound and CT. For validation of the tracking capabilities of the proposed framework, a 180×160×90 mm box was filled with a compound of 5 weight percent (wt%) gelatin and 1 wt% agar. Two plastic spheres of 40 mm diameter were submerged around 15 mm and 25 mm below the surface, respectively. After cooling, the box was rigidly attached to a second robot, KUKA LWR 4+ (KUKA Roboter GmbH, Augsburg, Germany), as shown in Fig. 5. The first robot was manually positioned such that the central US slice was parallel to the axis connecting both sphere centers. The poses of both robot end-effectors were recorded with 50 Hz. Because we aligned both robot coordinate systems by design and only considered relative translations and rotations in the horizontal plane (t_x, t_y, γ), no explicit robot-to-robot calibration was necessary. The three registration parameters were bound to ± 20 mm and $\pm 30°$ for each time step. The Cartesian stiffnesses of the impedance controller were set to 2,000 N/m (translation) and 400 Nm/rad (rotation) to avoid inaccuracies due to friction effects. The damping was 0.7 Ns/m.

B. Spine Phantom Validation

For lumbar spine needle insertions, we constructed a spine phantom similar to the one in [9]. A radiopaque spine phantom (L1 to sacrum; Sawbones, Pacific Research Laboratories Inc., Vashon Island, WA, USA) was embedded in a 380×240×150 mm box filled with a compound of 3.5 wt% gelatin and 0.7 wt% agar. On an isometric CT image with 1.25 mm resolution, insertion paths and needle targets were planned for two facet joint and two epidural injections. After an initial US scan following manual placement of the transducer and CT-to-US registration, the needle guide control scheme was used to manually insert 18-gauge needles to all four target sites. All inserted needles remained in the phantom and were fixed on the surface using thermoplastic adhesive. Placement accuracy was evaluated using manual annotations of the needle tip by an expert on a second CT scan, which was rigidly registered to the first one. We report the placement error e_p as the distance between the needle tip and the planned needle path. To mimic realistic conditions [30], we used a stiffness of 500 N/m and a desired force of $F_d = 5$ N, both expressed in needle direction.

V. RESULTS

A. Tracking Accuracy Validation

In a first set of experiments, the KUKA 4+ robot holding the phantom was moved by a series of translations (± 10 mm) and rotations ($\pm 20°$). As exemplarily shown in Fig. 4, all movements were successfully detected by the registration algorithm, allowing the visual servoing controller to compensate and realign the US transducer centrally over the phantom. The relative translation error $e_t = \left\| \vec{t}_{iiwa} - \vec{t}_{4+} \right\|$, measured as the difference between the relative movements of each robot after convergence of the visual servoing controller, was for $N = 10$ experiments 0.42 ± 0.44 mm (mean $\pm$ standard deviation). The rotational error $e_r = |\gamma_{iiwa} - \gamma_{4+}|$ was $0.39 \pm 0.50°$ ($N = 8$). While the controller reached the new pose on average after 3.32 seconds, oscillations were observed, and the average time until complete motionlessness was 8.75 seconds.

In a second experiment, we evaluated whether the registration drifts or is lost over time. The 4+ robot performed a continuous motion, translating the phantom in 180 seconds

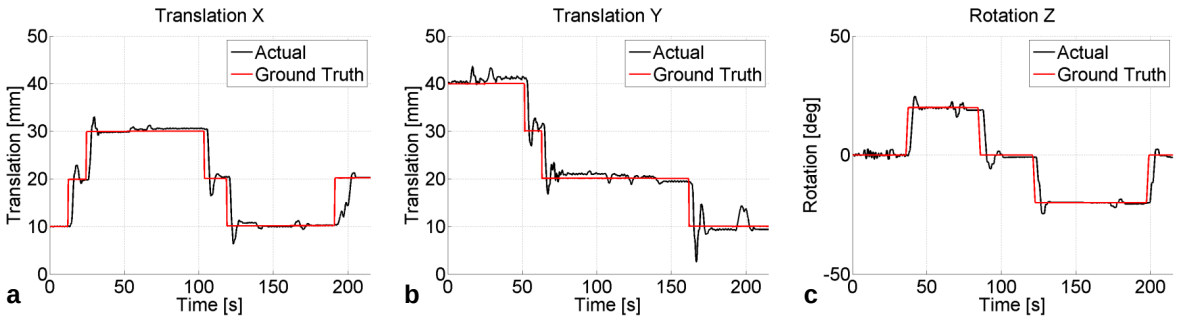

Fig. 4. System behavior during tracking accuracy experiments. Any movement of KUKA 4+ robot holding the phantom (± 10 mm or $\pm 20°$, respectively; *red line*) is detected by the visual servoing controller, and the KUKA iiwa robot holding the US transducer follows (*black line*).

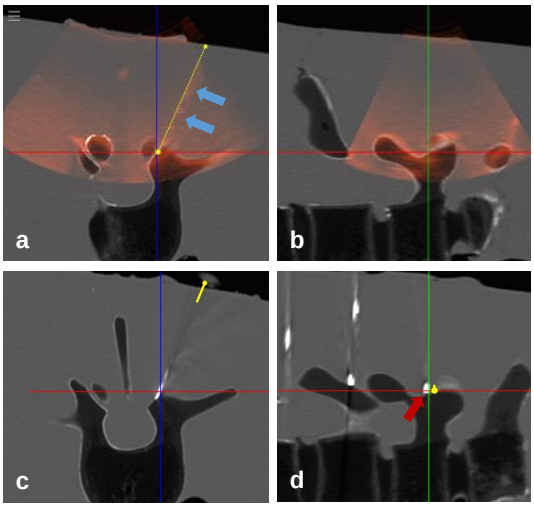

Fig. 6. **a, b)** During manual needle placement, our framework visualizes the live 3D ultrasound image (*red overlay*) and the registered pre-interventional CT image. The software orients the views automatically such that the needle guide line (*yellow*) is fully visible. Blue arrows indicate the echo of the already inserted needle. **c, d)** We validated our system with a CT image after all needles were inserted. The red arrow indicates the tip of the inserted needle, showing good agreement with the planned target site (*yellow*).

on circular path of 100 mm radius on the horizontal plane. The rotation with respect to the world frame F_w was fixed. Throughout the whole experiment, the distance of the US transducer to the center of the circle was 100.11 ± 0.66 mm. After one full rotation, the iiwa robot returned up to $\vec{t}_{iiwa} = 0.39$ mm to its original position.

B. Spine Phantom Validation

Fig. 6a-b demonstrate the live 3D ultrasound image as well as the registered pre-interventional CT image during guidance and needle placement at the L1-L2 facet joint. In Fig. 6c-d, slices of the confirmation CT image of the same needle are visualized. The errors of manual needle placement e_p for all four inserted needles are reported in Tab. I, amounting on average to 4.26 mm. Finally, a 3D rendering of the confirmation CT, including all placed needles and planned needle paths, is shown in Fig. 7.

TABLE I
MANUAL NEEDLE PLACEMENT ERRORS UNDER ROBOTIC GUIDANCE

Nr	Site	Error e_p [mm]
1	Facet joint L1-L2 left	3.41
2	Facet joint L2-L3 left	4.73
3	Epidural L2-L3	3.52
4	Epidural L3-L4	5.41

C. Computational Performance

The employed 3D volume update rate was 1.3 Hz. During acquisition of image I_i, the previous image I_{i-1} was processed in parallel. The compounding of the raw 2D frames into a 3D volume took on average 40 ms, the registration to the initial US volume between 400 and 500 ms. All processing steps could therefore be completed before the next volume acquisition was complete.

VI. DISCUSSION

The relative tracking errors obtained in our sphere phantom experiments illustrate that accurate tracking relative to an initial 3D image is possible, and that there is no drift of the tracking performance over time. This is particularly important in clinical scenarios requiring image guidance over longer durations. However, the time until complete convergence, i.e. motionlessness after target movement, is relatively high, even though compounding and registration are computed in parallel on GPU. In this regard, several factors can be considered to increase the rapidity of the system. First, the low 3D volume update rate clearly forms an obstacle. The utilization of 4D matrix US transducers or high frame rate technology [31] might solve this problem. Second, the registration itself could be potentially sped up by reducing the image size (downsampling) or by registering only parts of the involved images. A more extensive study is required to determine the influence of registration accuracy on the servoing behavior. Reducing the overall update rate of the system might also limit the oscillations (overshoots) observed after rapid movements, which are induced by the fact that while the robot is compensating, new (distorted) volumes are acquired. In the future, this effect could also be mitigated by using the current robot position for each individual US frame during compounding. Nevertheless, current limitations in the imaging rate do not restrict the usability of the proposed framework as the controller regularly recovers after few iterations, and the expected target movements in clinical routine are smaller than those evaluated in our experiments [30].

In robotically guided needle insertion experiments, promising placement errors were obtained. While the accuracy of our framework will need refinement for facet joint applications, the achieved precision in the two epidural insertions might already be sufficient for clinical use [32]. Yet, the needle placement accuracy is in the range of millimeters, most probably due to the long (100 mm) and not completely rigid needle in combination with a slight play in the needle guide, and the lack of needle tracking and bending compensation algorithms. In combination with shorter and more rigid needles as well as a more sophisticated needle guide, the inclusion of such algorithms has the potential to improve the overall accuracy of our system.

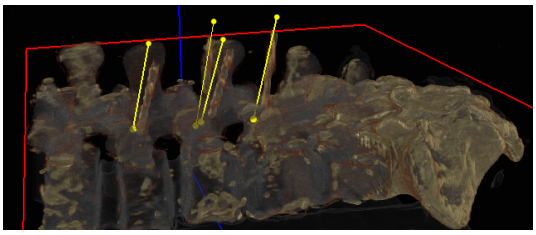

Fig. 7. 3D rendering of the CT image after needle placement, showing all four inserted needles and the planned needle paths.

VII. CONCLUSION

In this work, we presented an overall solution for interventional navigation based on multi-modal fusion to pre-interventional data, and a novel visual servoing framework that combines real-time image-based 3D ultrasound registration with real-time servo-control. In phantom experiments including a lumbar spine model, we have demonstrated that the proposed robotic system can accurately follow moving target anatomies and thus greatly support physicians in performing needle insertions. Our framework is generic and can potentially be employed in the future also to other interventions that require ultrasound guidance.

REFERENCES

[1] P. Center and L. Manchikanti, "A systematic review and best evidence synthesis of effectiveness of therapeutic facet joint interventions in managing chronic spinal pain," *Pain physician*, vol. 18, pp. E535–E582, 2015.

[2] S. H. Yoon, S. L. OBrien, and M. Tran, "Ultrasound guided spine injections: advancement over fluoroscopic guidance?" *Current Physical Medicine and Rehabilitation Reports*, vol. 1, no. 2, pp. 104–113, 2013.

[3] S.-A. Ahmadi, F. Milletari, N. Navab, M. Schuberth, A. Plate, and K. Bötzel, "3D transcranial ultrasound as a novel intra-operative imaging technique for DBS surgery: a feasibility study," *International Journal of Computer Assisted Radiology and Surgery*, pp. 1–10, 2015.

[4] S. B. Kesner and R. D. Howe, "Robotic catheter cardiac ablation combining ultrasound guidance and force control," *The International Journal of Robotics Research*, vol. 33, no. 4, pp. 631–644, 2014.

[5] G. R. de Oliveira Filho, "The construction of learning curves for basic skills in anesthetic procedures: an application for the cumulative sum method," *Anesthesia & Analgesia*, vol. 95, no. 2, pp. 411–416, 2002.

[6] J. Moore, C. Clarke, D. Bainbridge, C. Wedlake, A. Wiles, D. Pace, and T. Peters, "Image guidance for spinal facet injections using tracked ultrasound," in *Medical Image Computing and Computer-Assisted Intervention–MICCAI 2009*. Springer, 2009, pp. 516–523.

[7] D. Tran, A. A. Kamani, E. Al-Attas, V. A. Lessoway, S. Massey, and R. N. Rohling, "Single-operator real-time ultrasound-guidance to aim and insert a lumbar epidural needle," *Canadian Journal of Anesthesia/Journal canadien d'anesthésie*, vol. 57, no. 4, pp. 313–321, 2010.

[8] C. X. Yan, B. Goulet, J. Pelletier, S. J.-S. Chen, D. Tampieri, and D. L. Collins, "Towards accurate, robust and practical ultrasound-CT registration of vertebrae for image-guided spine surgery," *International Journal of Computer Assisted Radiology and Surgery*, vol. 6, no. 4, pp. 523–537, 2011.

[9] T. Ungi, P. Abolmaesumi, R. Jalal, M. Welch, I. Ayukawa, S. Nagpal, A. Lasso, M. Jaeger, D. P. Borschneck, G. Fichtinger, and P. Mousavi, "Spinal needle navigation by tracked ultrasound snapshots," *Biomedical Engineering, IEEE Transactions on*, vol. 59, no. 10, pp. 2766–2772, 2012.

[10] A. Rasoulian, J. Osborn, S. Sojoudi, S. Nouranian, V. A. Lessoway, R. N. Rohling, and P. Abolmaesumi, "A system for ultrasound-guided spinal injections: A feasibility study," in *Information Processing in Computer-Assisted Interventions*. Springer, 2014, pp. 90–99.

[11] M. Brudfors, A. Seitel, A. Rasoulian, A. Lasso, V. A. Lessoway, J. Osborn, A. Maki, R. N. Rohling, and P. Abolmaesumi, "Towards real-time, tracker-less 3D ultrasound guidance for spine anaesthesia," *International Journal of Computer Assisted Radiology and Surgery*, pp. 1–11, 2015.

[12] P. Abolmaesumi, S. Salcudean, and W. Zhu, "Visual servoing for robot-assisted diagnostic ultrasound," in *Engineering in Medicine and Biology Society, 2000. Proceedings of the 22nd Annual International Conference of the IEEE*, vol. 4. IEEE, 2000, pp. 2532–2535.

[13] R. Nakadate, J. Solis, A. Takanishi, E. Minagawa, M. Sugawara, and K. Niki, "Out-of-plane visual servoing method for tracking the carotid artery with a robot-assisted ultrasound diagnostic system," in *Robotics and Automation (ICRA), 2011 IEEE International Conference on*. IEEE, 2011, pp. 5267–5272.

[14] C. Nadeau and A. Krupa, "Intensity-based ultrasound visual servoing: Modeling and validation with 2-D and 3-D probes," *Robotics, IEEE Transactions on*, vol. 29, no. 4, pp. 1003–1015, 2013.

[15] A. Krupa, D. Folio, C. Novales, P. Vieyres, and T. Li, "Robotized tele-echography: an assisting visibility tool to support expert diagnostic," *Systems Journal, IEEE*, no. 99, pp. 1 – 10, 2014.

[16] T. Idzenga, E. Gaburov, W. Vermin, J. Menssen, and C. De Korte, "Fast 2-D ultrasound strain imaging: the benefits of using a GPU," *Ultrasonics, Ferroelectrics, and Frequency Control, IEEE Transactions on*, vol. 61, no. 1, pp. 207–213, 2014.

[17] T. K. Adebar, A. E. Fletcher, and A. M. Okamura, "3-D Ultrasound-Guided Robotic Needle Steering in Biological Tissue," *Biomedical Engineering, IEEE Transactions on*, vol. 61, no. 12, pp. 2899–2910, 2014.

[18] A. Krupa, "3D steering of a flexible needle by visual servoing," in *Medical Image Computing and Computer-Assisted Intervention–MICCAI 2014*. Springer, 2014, pp. 480–487.

[19] C. Nadeau, H. Ren, A. Krupa, and P. Dupont, "Intensity-based visual servoing for instrument and tissue tracking in 3D ultrasound volumes," *Automation Science and Engineering, IEEE Transactions on*, vol. 12, no. 1, pp. 367–371, 2015.

[20] A. Albu-Schäffer, C. Ott, U. Frese, and G. Hirzinger, "Cartesian impedance control of redundant robots: Recent results with the DLR-light-weight-arms," in *Robotics and Automation, 2003. Proceedings. ICRA'03. IEEE International Conference on*, vol. 3. IEEE, 2003, pp. 3704–3709.

[21] W. Wein, S. Brunke, A. Khamene, M. R. Callstrom, and N. Navab, "Automatic CT-ultrasound registration for diagnostic imaging and image-guided intervention," *Medical Image analysis*, vol. 12, no. 5, pp. 577–585, 2008.

[22] M. J. Powell, "The BOBYQA algorithm for bound constrained optimization without derivatives," *Cambridge NA Report NA2009/06, University of Cambridge, Cambridge*, 2009.

[23] B. Fuerst, W. Wein, M. Müller, and N. Navab, "Automatic ultrasound–MRI registration for neurosurgery using the 2D and 3D LC2 metric," *Medical Image Analysis*, vol. 18, no. 8, pp. 1312–1319, 2014.

[24] P. Malenfant, V. Gunka, P. Beigi, A. Rasoulian, R. Rohling, and A. Dube, "Accuracy of 3D ultrasound for identification of epidural needle skin insertion point in parturients; a prospective observational study," in *Society for obstetric anesthesia and perinatology (SOAP) 46th annual meeting, Toronto, ON, Canada*, 2014, p. 308.

[25] S. Tauscher, J. Tokuda, G. Schreiber, T. Neff, N. Hata, and T. Ortmaier, "OpenIGTLink interface for state control and visualisation of a robot for image-guided therapy systems," *International journal of computer assisted radiology and surgery*, vol. 10, no. 3, pp. 285–292, 2015.

[26] A. Lasso, T. Heffter, A. Rankin, C. Pinter, T. Ungi, and G. Fichtinger, "PLUS: Open-source toolkit for ultrasound-guided intervention systems," *IEEE Transactions on Biomedical Engineering*, no. 10, pp. 2527–2537, Oct 2014.

[27] J. Tokuda, G. S. Fischer, X. Papademetris, Z. Yaniv, L. Ibanez, P. Cheng, H. Liu, J. Blevins, J. Arata, A. J. Golby, T. Kapur, S. Pieper, E. C. Burdette, G. Fichtinger, C. M. Tempany, and N. Hata, "OpenIGTLink: an open network protocol for image-guided therapy environment," *The International Journal of Medical Robotics and Computer Assisted Surgery*, vol. 5, no. 4, pp. 423–434, 2009.

[28] A. Karamalis, W. Wein, O. Kutter, and N. Navab, "Fast hybrid freehand ultrasound volume reconstruction," in *SPIE Medical Imaging*. International Society for Optics and Photonics, 2009, pp. 726 114–726 114.

[29] J. Dang, B. Frisch, P. Lasaygues, D. Zhang, S. Tavernier, N. Felix, P. Lecoq, E. Auffray, J. Varela, S. Mensah, and M. Wan, "Development of an anthropomorphic breast phantom for combined PET, B-mode ultrasound and elastographic imaging," *Nuclear Science, IEEE Transactions on*, vol. 58, no. 3, pp. 660–667, 2011.

[30] N. Smith-Guerin, L. A. Bassit, G. Poisson, C. Delgorge, P. Arbeille, and P. Vieyres, "Clinical validation of a mobile patient-expert tele-echography system using ISDN lines," in *Information Technology Applications in Biomedicine, 2003. 4th International IEEE EMBS Special Topic Conference on*. IEEE, 2003, pp. 23–26.

[31] J. Provost, C. Papadacci, J. E. Arango, M. Imbault, M. Fink, J.-L. Gennisson, M. Tanter, and M. Pernot, "3D ultrafast ultrasound imaging in vivo," *Physics in Medicine and biology*, vol. 59, no. 19, p. L1, 2014.

[32] J. Kessler, B. Moriggl, and T. Grau, "The use of ultrasound improves the accuracy of epidural needle placement in cadavers," *Surgical and Radiologic Anatomy*, vol. 36, no. 7, pp. 695–703, 2014.